Nondestructive Surface Profiling and Inspection by Using a Single Unit **Magneto-Eddy-Current Sensor**

Jungsub Kim

J. Mike Walker '66 Department of Mechanical Engineering, Texas A&M University,

3123 TAMU, College Station, TX 77843-3123 e-mail: poiu0513@tamu.edu

Heebum Chun

J. Mike Walker '66 Department of Mechanical Engineering, Texas A&M University,

3123 TAMU, College Station, TX 77843-3123

e-mail: hchun@tamu.edu

ChaBum Lee

J. Mike Walker '66 Department of Mechanical Engineering, Texas A&M University,

3123 TAMU, College Station, TX 77843-3123

e-mail: cblee@tamu.edu

This paper presents a novel nondestructive testing system, magnetoeddy-current sensor (MECS), to enable surface profiling of dissimilar materials by combining magnetic sensing for ferromagnetic materials and eddy-current sensing for nonferromagnetic materials. The interactions between an electromagnetic field and nonferromagnetic surface and between a magnetic field and ferromagnetic surface were measured by the MECS. The MECS consists of a conic neodymium magnet and a copper coil wound around the magnet. Aluminum and steel surfaces bonded together were prepared to test nondestructive surface profiling of dissimilar materials by the MECS. The interactions between an electromagnetic field and aluminum surface were characterized by monitoring the impedance of the coil, and the interactions between a magnetic field and steel surface were characterized by using a force sensor attached to the neodymium magnet. The magnetic and electromagnetic effects were numerically analyzed by the finite element model. The developed MECS showed the following performance: measurement spot size 5 mm and 10 mm, dynamic measurement bandwidth (eddy-current sensing 1 kHz and magnetic sensing 200 Hz), measuring range 25 mm and 17 mm, polynomial fitting error 0.51% and 0.50%, and resolution 0.655 µm and 0.782 µm for nonferromagnetic and ferromagnetic surface profiling, respectively. This technique was also applied to surface profiling and inspection of the rivet joining sheet materials. The results showed that the MECS is capable of nondestructively monitoring and determining the riveting quality in a fast, large-area, low-cost, convenient manner. [DOI: 10.1115/1.4053810]

Keywords: nondestructive testing, eddy-current sensor, magnetic sensor, surface profiling, metrology, sensing, monitoring and diagnostics, sensors

1 Introduction

Surface profile measurement and inspection technique is of importance for quantifying the surface quality of the machined parts. Surface profile error, including form error, waviness, and

roughness, must be compensated to achieve the desired surface quality of the parts. There are few surface profiling instruments for noncontact or nondestructive, large-range, fast, low-cost applications. Atomic force microscopy, white light interferometry, confocal microscopy, etc. are typically used for high-precision parts such as lenses, mirrors, and gratings [1-3], and the other parts can be easily measured by coordinate measuring machines (CMM), dial gauges, linear variable differential transformer (LVDT), and so on [4-6]. However, those measuring methods are not capable of surface profiling of the inner layer of the parts such as dissimilar materials bonded with two different materials. Necessarily, the destructive methods such as removing the outer layer of the parts or slicing the parts are obliged to be adapted, or nondestructive surface profiling methods including industrial X-ray computed tomography (CT) scan [7,8], magnetic resonance imaging [9], ultrasonic measurement [10], eddy-current sensing [11–15], and capacitive sensing [16,17] are often used.

Dissimilar materials bonded along with two or more sheets of materials such as aluminum alloys, steels, or even composites have been widely used in aerospace, automotive, and shipbuilding industries to make the structures lighter, stronger, and more costeffective [18–20]. Some defects that occur during the production process can lead to subsequent quality problems and increase production cost and risk. Typical defects during the production process are wrinkles, missing bundles, misalignment, cracks, delamination, impact damages, and so on [21]. Therefore, a few nondestructive methods mentioned earlier are used to inspect the defects and to guarantee quality and reliability. Kim et al. [22] introduced a nondestructive volumetric thickness profile measurement method for transparent thin film by optical scanning. But this method is difficult to implement into the production process earlier. Stepinski et al. introduced ultrasonic spectroscopy for layered structures and self-piercing rivets (SPR) [23,24]. However, it limits to provide information on the location of the defect. Johnson et al. [25] reported X-ray CT scan and computer vision techniques to visualize the geometrical quality features of the SPR joints. But the inspection speed is slow for monitoring and there is a large volume to be inspected. And those methods take a long time, are expensive, and are only capable of small-area measurements. Therefore, there are technological gaps in nondestructive surface profile measuring methods capable of large-area in-line scanning in a fast, reliable, low-cost manner.

In this study, a novel nondestructive surface profiling and inspection technique capable of dissimilar materials was proposed, and the single unit sensor unit for both eddy-current sensing and magnetic force measurement was developed and tested. The electromechanical interactions between the measurement unit and ferromagnetic and nonferromagnetic target materials were measured precisely. The measurement principles, sensor design, calibration, and performance test results were discussed.

2 Sensor Design and Implementation

To design and characterize the magnetic and eddy-current effects, finite element analysis (FEA) was first conducted by using a Maxwell software package. A magneto-eddy-current sensor (MECS) consists of a conic neodymium (N48) magnet having a top diameter of 12.7 mm, a bottom diameter of 1.2 mm, and a height of 12.7 mm, and a copper wire of Ø0.3 mm was modeled and was simulated to compare the case of the magnet with wound copper coil and the case of the magnet without wound copper coil. A rectangular steel plate (100 mm × 10 mm) as a measurement target was employed to measure the attractive force between the magnet and the target. For the simulations, the magnetic properties of the N48 magnet, copper, and steel were used as input parameters to perform the FEA. The magnet was set a north magnetic pole and a south magnetic pole at the top and the bottom, respectively. In order not to affect each other between the magnetic flux and strength of magnet and the magnetic flux and strength of

¹Corresponding author.

Manuscript received October 28, 2021; final manuscript received February 3, 2022; published online April 9, 2024. Assoc. Editor: Chinedum Okwudire.

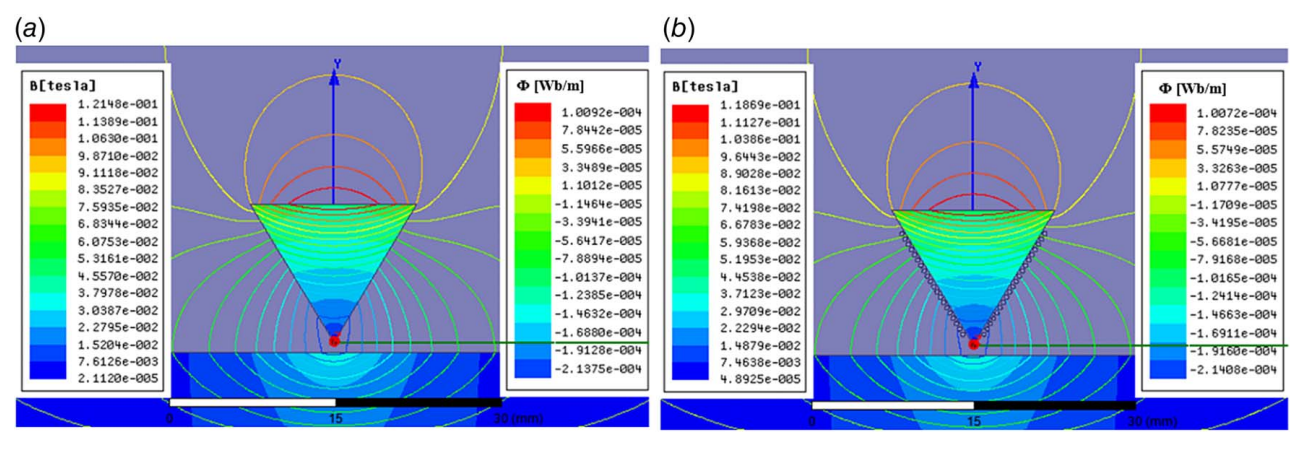


Fig. 1 The distribution of the magnetic strength B and flux Φ : (a) magnet without wound copper coil and (b) magnet with wound copper coil

electromagnet, current 0.1 A was supplied to the copper wire. The rectangular steel plate was fixed, and the attractive force of the magnet was obtained between the tip of the magnet from the rectangular steel at a gap distance of 0.2, 0.4, 0.6, 0.8, and 1.0 mm. The complete FEA model was composed of 154,284 elements. Figure 1 shows the resultant magnetic field strength B (gradient) and magnetic flux Φ (contour). The case of the magnet with wound copper coil and the case of the magnet without wound copper coil showed a similar resultant magnetic field strength and magnetic flux according to the gap distances between the tip of a conic magnet from the rectangular steel plate. Figure 1(b) shows the resultant magnetic field distribution according to the magnet and electromagnet effects, and Fig. 2 shows the force distribution to the gap distance. The force distribution over 1 mm gap distance showed less than 0.25% difference between with and without the electromagnetic effect by the coil, and the electromagnetic effect on the magnetic force against the steel plate was too small to consider compared with the permanent magnet effect. This result shows that crosstalk between the permanent magnet effect and electromagnetic effect is negligible, so the effects of magnet and eddy current are independent.

The single unit MECS that measures the interactions between an electromagnetic field and nonferromagnetic surface and between a magnetic field and ferromagnetic surface was designed and

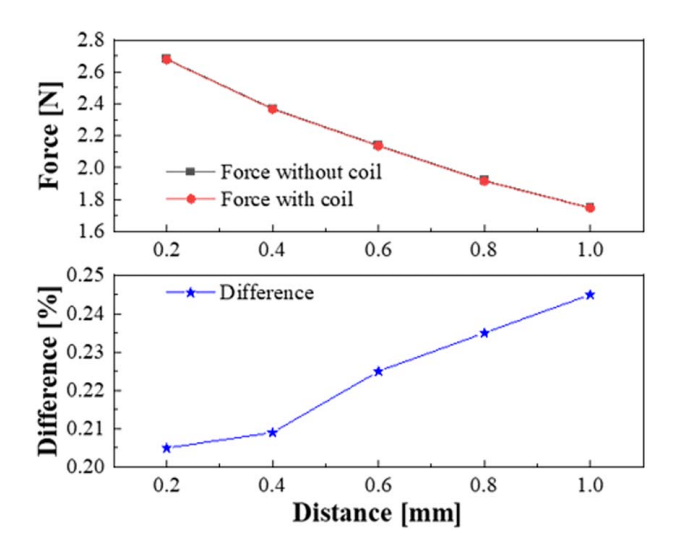


Fig. 2 The attractive force of the magnet without wound copper coil and the magnet with wound copper coil according to the target distance

fabricated to enable surface profiling of the respective surface of nonferromagnetic and ferromagnetic dissimilar material. The schematic diagram of the MECS is shown in Fig. 3. The MECS consisted of a conic neodymium magnet of ø12.7 mm (grade N48), a three-axis load cell as force sensor (FNZ-10N, Forsentek, Guangdong, China), an amplifier (LC4A, Forsentek), a copper wire (28AWG), a lock-in amplifier (SR833, SRS, USA), and a function generator (33120A, Agilent, Santa Clara, CA). For scanning the ferromagnetic surface of nonferromagnetic and ferromagnetic dissimilar material, the force sensor with the conic neodymium magnet attached was used to measure the interaction between the magnetic field and the ferromagnetic surface. The conic neodymium magnet having a sharp tip was selected to increase the resolution of the sensor. The force sensor is based on an electrical circuit called Wheatstone bridge. The circuit allows to measure very small changes in the resistance, which occurs in the strain gauges placed in the arms of the bridge $(R_1, R_2, R_3, R_4 \text{ in Fig. } 3(b))$. The attractive force that deforms strain gauges in the force sensor will produce a change of resistance. The resistance change on each strain gauge is magnified by the imbalance produced in the bridge and thus obtains an output signal proportional to the attractive force. And the copper wire was wound 20 turns around the conic neodymium magnet and current 0.1 A was supplied for eddy-current sensing. The copper wire formed an eddy current to scan the nonferromagnetic surface of nonferromagnetic and ferromagnetic dissimilar material to sense the interaction of the electromagnetic field between the probe and target surface. And the lock-in amplifier and the function generator were employed for the amplitude modulation to increase the sensor sensitivity of eddy current. The modulation signal has an amplitude of 1 V and a frequency of 100 kHz sine waveform. The eddy-current sensor has a series of inductor–resistor (LR) circuit based on the lossy inductor model. Both inductance, coil, and resistance, R3, change with distance from the target. As the target approaches the coil, the inductance goes down and the resistance usually goes up. The change in inductance provides an output signal for detecting the target. As a result, the magneto of the conic neodymium magnet and the eddy current of the copper wire can nondestructively and simultaneously scan the surfaces of nonferromagnetic aluminum and ferromagnetic steel. In the MECS, the force sensor is based on strain gauges that the bandwidth is limited to 200 Hz. The eddycurrent sensor has a low-pass filter (LPF) with a cut of frequency 1000 Hz at the end of the circuit because high bandwidth causes high sensor noise. Those bandwidths were determined based on the speed of the scanning units. Typically, the surface profiling probes have a low measurement bandwidth because a system does not measure the moving targets but the stationary ones. Thus, the dynamic measurement limit of the MECS depends on the bandwidth of the force sensor and the eddy-current sensor. Therefore, the MECS has a bandwidth of 200 Hz.

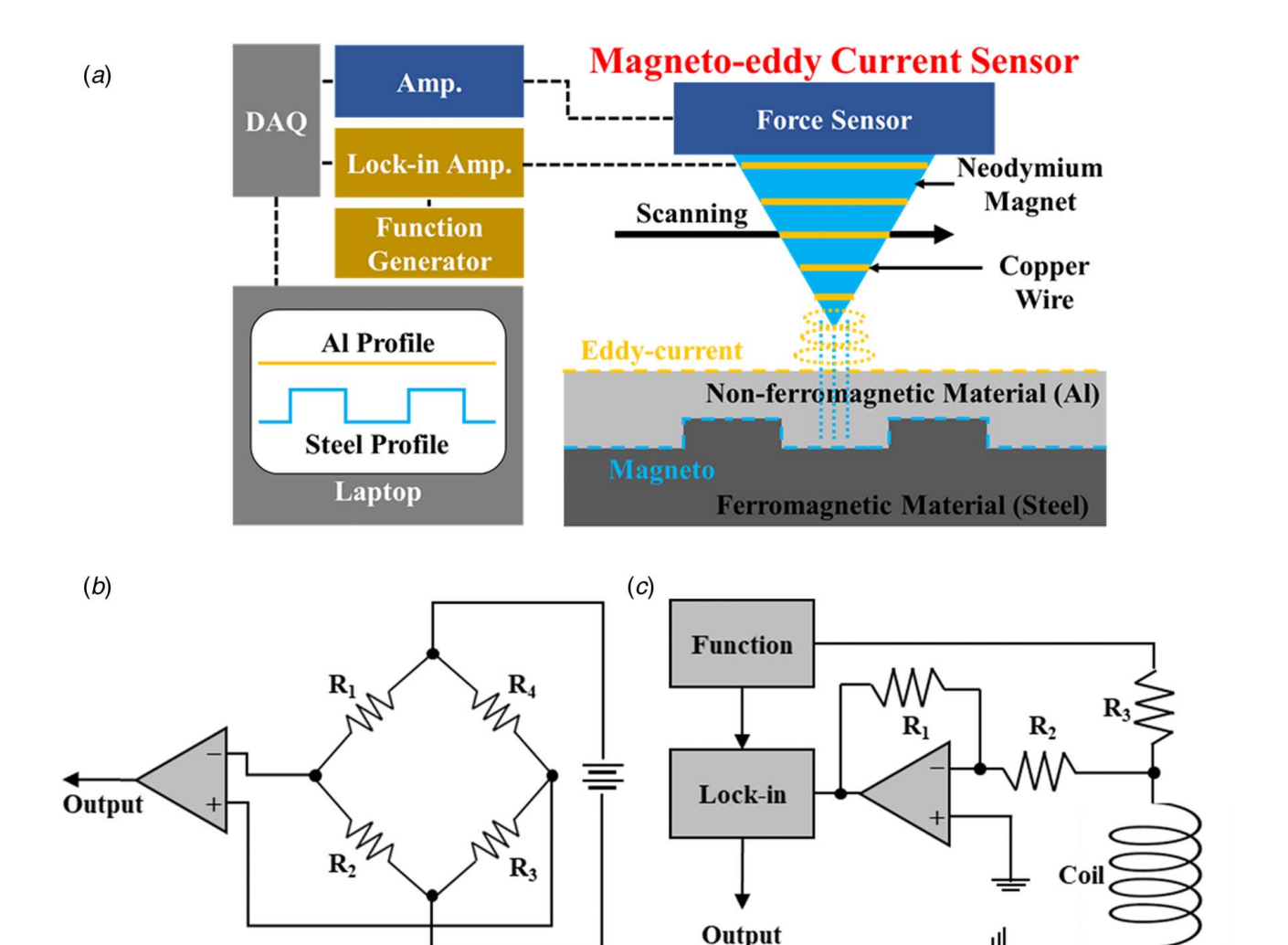


Fig. 3 Schematic diagrams: (a) entire system, (b) force sensor, and (c) eddy-current sensor

3 Experiments

The scanning system was constructed to scan the samples as shown in Fig. 4. A high-precision linear stage with 10 nm positioning control resolution was used to scan the sample. The MECS probe was attached to a two-axis linear stage to control the *z*- and

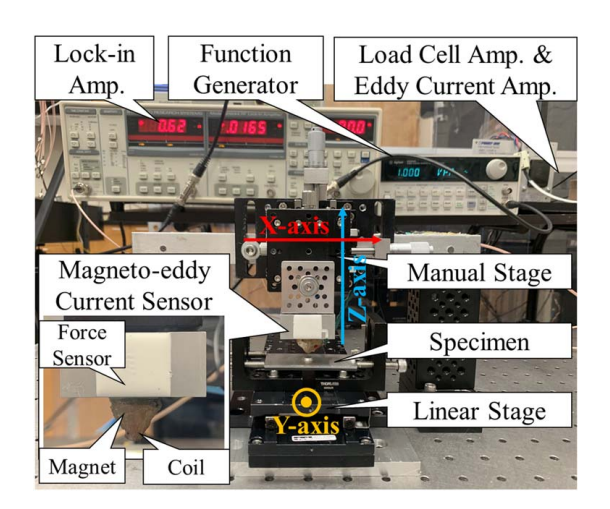


Fig. 4 MECS-based scanning system

x-axis feed. The specimen was placed on the linear stage for scanning the specimens along the *y*-axis, and the motor controller was connected to the linear stage to control the position of the linear stage. The surface profiles of dissimilar materials were measured by the MECS. To confirm the performance of the MECS, the steel-flat plate (permeability $\mu 2.5 \times 10^{-1}$ H/m, electric conductivity $\sigma 10.1 \times 10^{+6}$ S/m), aluminum plate ($\mu 1.26 \times 10^{-6}$ H/m, $\sigma 36.9 \times 10^{+6}$ S/m), and copper film ($\mu 1.26 \times 10^{-6}$ H/m, $\sigma 58.7 \times 10^{+6}$ S/m) were prepared and these samples sizes were a width of 30 mm, a length of 50 mm, and a height of 2 mm. The standard penetration depth δ at which the eddy-current density decreases in magnitude of 1/*e* was calculated according to the target materials by using the following equation [23]:

$$\delta = \frac{1}{\sqrt{\pi f \mu \sigma}} \tag{1}$$

Eddy-current

where f is the frequency. At f 100 kHz, the standard penetration depth was found approximately 1 μ m, 211 μ m, and 259 μ m for steel, copper, and aluminum, respectively. The magnetic sensing part was calibrated with the steel plate, and the eddy-current sensing part was calibrated with the copper surface. The steel-flat plate of 2 mm thickness with the copper film of 30 μ m thickness attached to the surface was fabricated as the specimen, and the MECS was calibrated by moving the linear stage along the z-axis. As shown in Fig. 5(a), the results showed that the MECS has polynomial fitting errors of 0.51% (magneto) and 0.50% (eddy-current) in the measuring range of 25 mm (magneto) and 17 mm

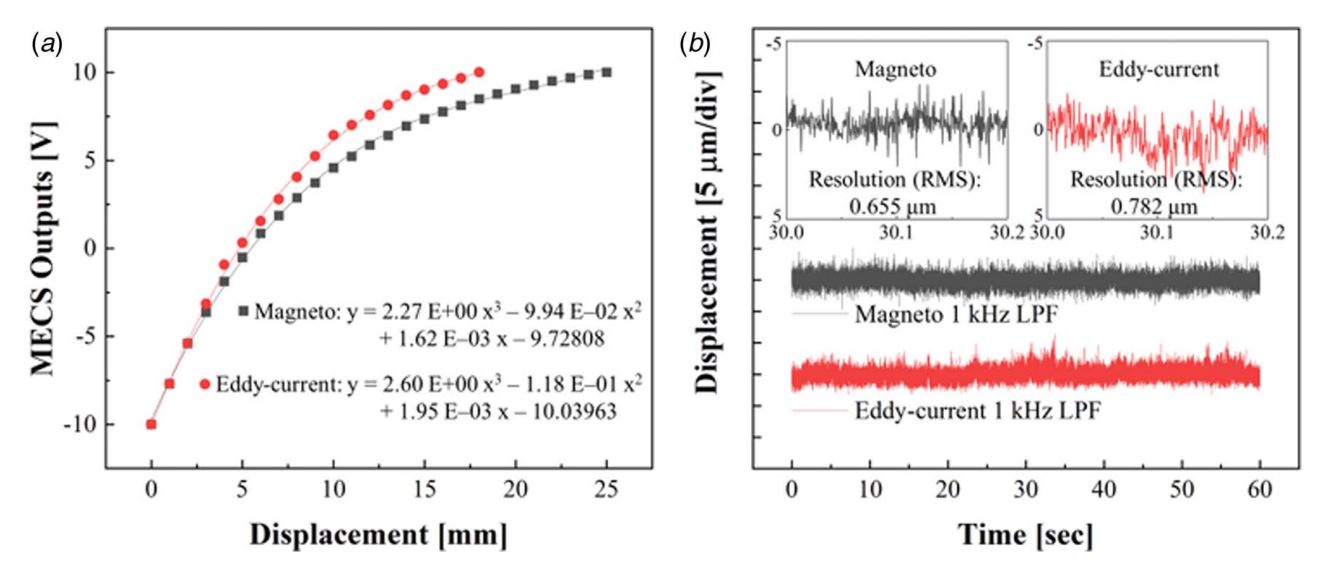


Fig. 5 MECS performance: (a) calibration curves and (b) noise level (1 kHz LPF was applied)

(eddy-current), respectively. Also, the noise level was estimated at a scanning distance of 1 μ m and a bandwidth of 10 kHz while the target sample was not in motion, root-mean-square values approximately 0.655 μ m (magneto) and 0.782 μ m (eddy-current) for ferromagnetic and nonferromagnetic surfaces, respectively, as shown in Fig. 5(b). These values could be considered as an axial resolution of the MECS.

4 Results

The two-dimensional (2D) scanning experiments were performed to obtain three-dimensional (3D) surface profiles of the target for performance verification of the MECS. For ferromagnetic surface profiling (magneto) using the MECS, one target sample was prepared by adding the steel washers (outer diameter of 20 mm, the inner diameter of 10 mm, and height of 2 mm) to the aluminum plate (width of 100 mm, length of 50 mm, and height of 2 mm). And the other target sample with 2 mm step height was prepared for nonferromagnetic surface profiling (eddy-current). The profiles of target samples were obtained by scanning the target samples

along the y-axis under scanning conditions: scanning speed 1 mm/s and scanning distance $100 \,\mu\text{m}$ (Fig. 6(a)) and $10 \,\text{mm}$ (Fig. 6(b)). Figure 6(a) shows that the magnetic sensor measures the steel washers' rim thickness (5 mm). Also, Fig. 6(b) shows that the eddy-current sensor measures a stepwise target with a 20 mm interval and a 2 mm height. As shown in Fig. 6, the obtained profiles of target samples were compared with those measured by Vernier caliper (500-196-30, Mitutoyo, Japan) and a commercial eddy-current sensor (U25 & ECA101, Lion precision, USA). These results showed that the profiles of target samples were successfully measured. The profiles of the target sample obtained by the MECS showed similar results to the profiles of target samples by the Vernier caliper and commercial eddy-current sensor over the full range. In Fig. 6(a), the result of ferromagnetic surface profiling (magneto) of the MECS showed the double lobes of the washer under the aluminum plate. This means that the MECS can perform nondestructive testing of samples composed of ferromagnetic and nonferromagnetic materials. In Fig. 6(b), the result of the nonferromagnetic surface profiling (eddy-current) of the MECS showed higher similarities than the result of the commercial eddy-current sensor. From the sensor noise results (Fig. 5(b)), the

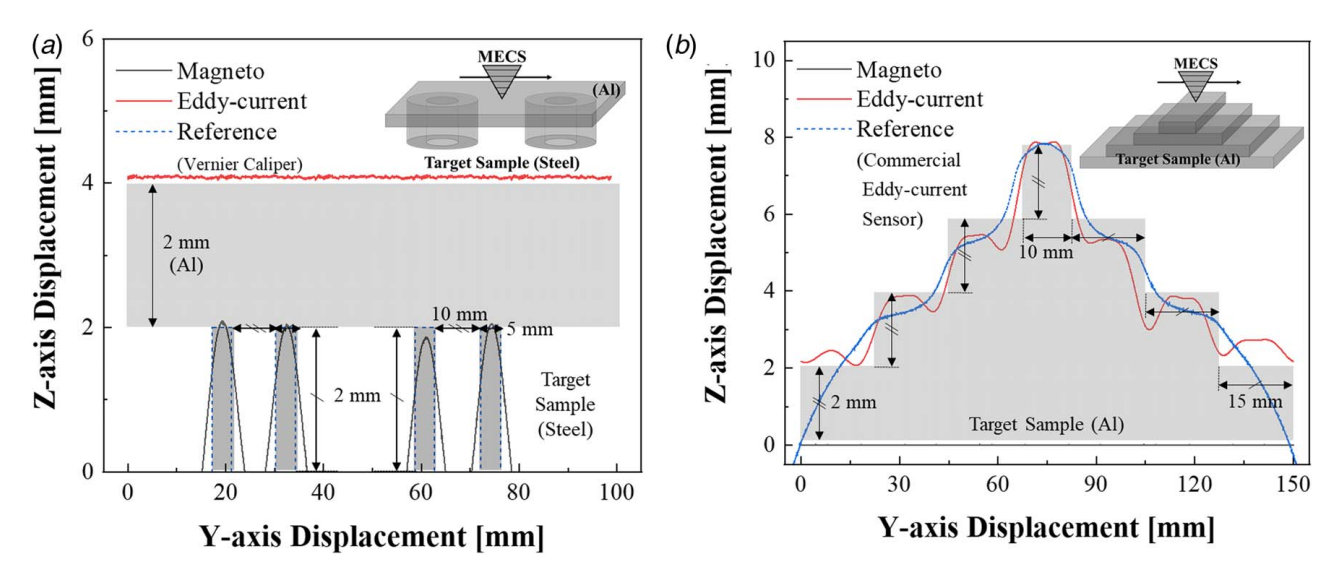


Fig. 6 2D scanning experiments using the MECS: (a) ferromagnetic surface profiling (magneto) and (b) nonferromagnetic surface profiling (eddy-current)

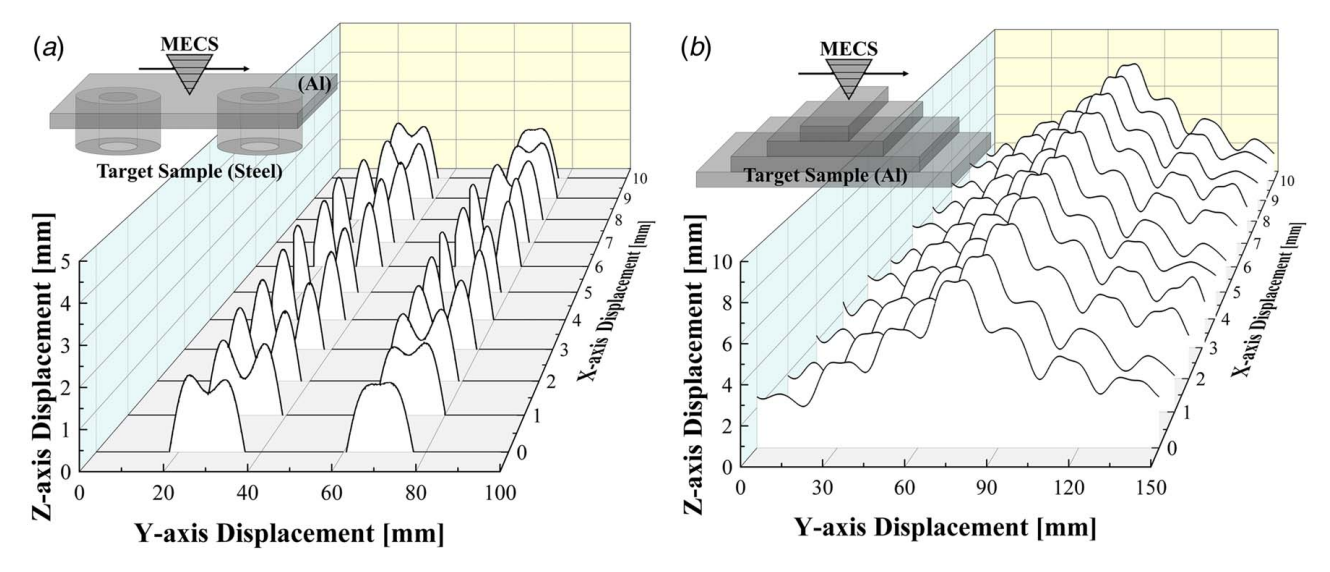


Fig. 7 3D scanning experiments using the MECS: (a) ferromagnetic surface profiling (magneto) and (b) nonferromagnetic surface profiling (eddy-current)

axial resolution of the MECS is approximately $0.655~\mu m$ for the ferromagnetic surface measurement and $0.782~\mu m$ for the nonferromagnetic surface measurement. From the surface scanning results (Fig. 6), the lateral resolution of the MECS is approximately 5 mm for the ferromagnetic surface measurement and 20 mm for the nonferromagnetic surface measurement.

In addition, the 3D scanning experiments were also conducted by scanning the target samples. The 3D scanning experiments were performed under the scanning conditions: scanning speed 1 mm/s and scanning distance $100 \, \mu m$ (Fig. 7(a)) and $10 \, mm$ (Fig. 7(b)). As the result, the 3D surface profiles of the target samples were reconstructed as seen in Fig. 7. Although the resolution of the MECS is lower than that of the commercial 3D scanning system, it is very attractive for industrial applications because it enables nondestructive testing.

In addition to the validation testing of the MECS, commercially available SPR was scanned by the MECS for nondestructive defect inspection. The SPR is formed by a cold mechanical

joining process that drives a rivet piercing through the materials. During the SPR process, the spreading of the rivet skirt is guided by a suitable die, and the punched slug from the top sheet or the top and middle sheets is embedded into the rivet cavity. Therefore, the SPR can fasten a variety of dissimilar materials, including steel, aluminum, polymer, carbon fiber reinforced polymer (CFRP), and so on [19,20,26–28]. The SPR may incur various defects including lack of interlock, asymmetry of rivet foot, buckling of the rivet, and so on. The defects affect the quality of joining part, which is critical to overall safety and cost. But there is a lack of a suitable nondestructive testing method for assessing the quality of the SPR [29].

Therefore, this study applies SPR surface profiling to detect the defect of the SPR. The specimens were prepared by the SPR process using an aluminum plate, the CFRP plate, and a steel rivet. The height of the aluminum plate and the CFRP plate was 2.00 mm and 1.80 mm, respectively. And the steel rivet of C-type and the FM-die were used to join the aluminum plate and the

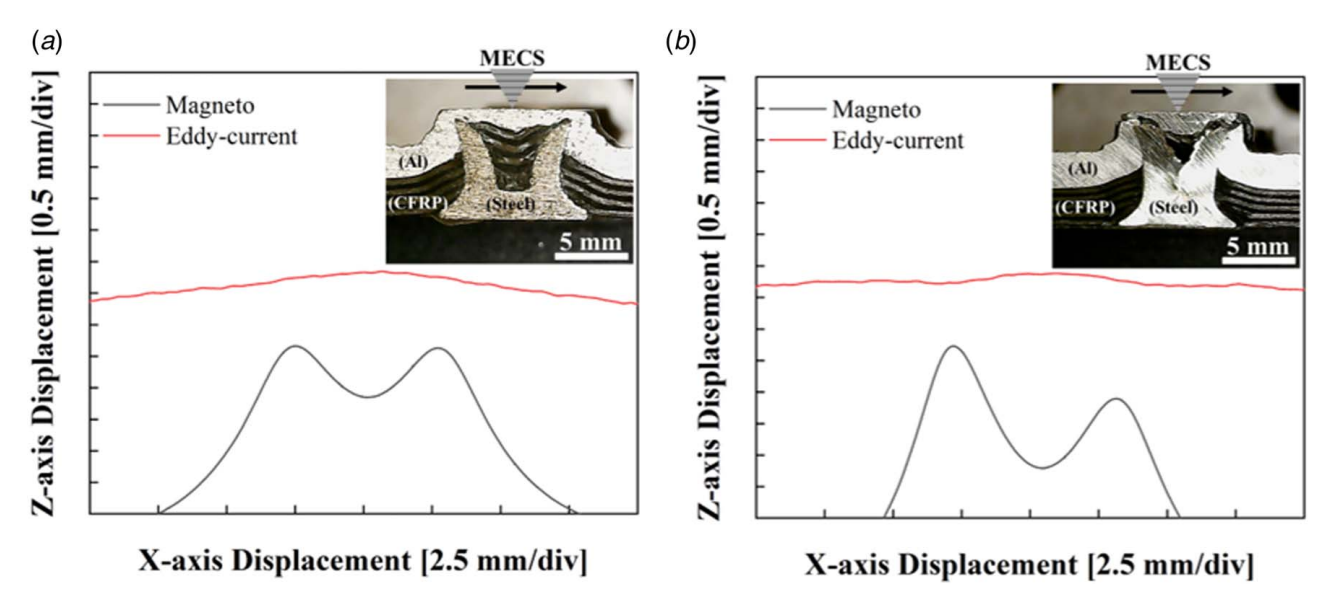


Fig. 8 SPR scanning results by using the MECS: (a) normal specimen and (b) abnormal specimen of the SPR. In general, the rivet in a normal SPR process is placed axis symmetric along the centerline and has a uniform gap thickness between the interlocking area and the aluminum top surface.

CFRP plate. To produce the specimens, the SPR system (GEN 2, Bolhoff, Troy, MI) was employed at a punching force of 50 kN, and then, the produced specimens were classified into normal specimens without penetrated crack and abnormal specimens with penetrated crack. The penetrated crack is one of the factors that diagnose the quality of the SPR [27]. And due to the penetrated crack, the bottom thickness is a factor for diagnosing the normal and abnormal specimens. Each specimen was measured by the scanning system under scanning conditions: a scanning speed of 1 mm/s. As shown in Fig. 8, the profiles of the aluminum plate (eddy-current) and steel rivet (magneto) of the SPR were obtained by the MECS, and the information of bottom thickness could be estimated using the profiles. In the abnormal SPR sample, the rivet was not placed axis symmetric along the centerline, and the gap distance between the rivet interlocking area and the aluminum top surface is not uniform. Although the rivet profile was not fully measured, the interlocking distance, rivet placement, and gap thickness were successfully measured by the MECS. Those results showed the potential to distinguish between normal and abnormal conditions of the SPR specimen and to detect the defect of the SPR specimen available for nondestructive SPR quality assessments.

5 Conclusion

In this study, the single unit MECS consisted of the magnetic sensor and eddy-current sensor was developed and was successfully implemented for nondestructive surface profiling and inspection of dissimilar materials. FEA results showed that crosstalk between the permanent magnet effect and the electromagnetic effect was negligibly small, which indicates that the two effects are independent. The signal processing technique is applied to improve the signal-to-noise of measurement systems. As a result, combining the magnetic sensor with the electromagnetic sensor in a single unit was effective to nondestructively measure both ferromagnetic and nonferromagnetic surface information and to inspect their defect modes. The scanning system for the MECS was constructed, and the scanning system was tested by precisely scanning several target samples. The MECS results were validated by using commercial measuring instruments. In addition, the MECS scanned the surface profile of the SPR samples. The results showed the MECS nondestructively measured the surface profiles of the SPR samples in a convenient, low-cost, fast, reliable manner, and showed the potential for nondestructive quality inspection of the SPR specimen as an alternative quality inspection system.

Acknowledgment

This research has been supported by Ministry of Trade, Industry and Energy (KEIT, Project No. 20011498, Robotic CFRP-metal mechanical joining and adhesive bonding process for future automotive applications).

Conflict of Interest

There are no conflicts of interest.

Data Availability Statement

The datasets generated and supporting the findings of this article are obtainable from the corresponding author upon reasonable request.

References

 Martin, Y., Williams, C. C., and Wickramasinghe, H. K., 1987, "Atomic Force Microscope—Force Mapping and Profiling on a sub-100-Å Scale," J. Appl. Phys., 61(10), pp. 4723–4729.

- [2] Deck, L., and De Groot, P., 1994, "High-Speed Noncontact Profiler Based on Scanning White-Light Interferometry," Appl. Opt., 33(31), pp. 7334–7338.
- [3] Udupa, G., Singaperumal, M., Sirohi, R. S., and Kothiyal, M. P., 2000, "Characterization of Surface Topography by Confocal Microscopy: I. Principles and the Measurement System," Meas. Sci. Technol., 11(3), pp. 305–314.
- [4] Hocken, R. J., and Pereira, P. H. 2012," Coordinate Measuring Machines and Systems, Vol. 6, CRC Press, Boca Raton, FL.
- [5] Keller, K., and Bonner, B. P., 1985, "Automatic, Digital System for Profiling Rough Surfaces," Rev. Sci. Instrum., 56(2), pp. 330–331.
- [6] Meydan, T., and Healey, G. W., 1992, "Linear Variable Differential Transformer (LVDT): Linear Displacement Transducer Utilizing Ferromagnetic Amorphous Metallic Glass Ribbons," Sens. Actuators, A, 32(1–3), pp. 582–587.
- [7] Hanke, R., Fuchs, T., and Uhlmann, N., 2008, "X-Ray Based Methods for Non-Destructive Testing and Material Characterization," Nucl. Instrum. Methods Phys. Res. A, 591(1), pp. 14–18.
- [8] Rathore, J. S., Mang, C., Vienne, C., Quinsat, Y., and Tournier, C., 2021, "A Methodology for Computed Tomography-Based Non-Destructive Geometrical Evaluations of Lattice Structures by Holistic Strut Measurement Approach," ASME J. Manuf. Sci. Eng., 143(5), p. 051012.
- [9] Lustig, M., Donoho, D. L., Santos, J. M., and Pauly, J. M., 2008, "Compressed Sensing MRI," IEEE Signal Process. Mag., 25(2), pp. 72–82.
- [10] Cawley, P., 1994, "The Rapid Non-Destructive Inspection of Large Composite Structures," Composites, 25(5), pp. 351–357.
- [11] Yu, Z., Fu, Y., Jiang, L., and Yang, F., 2021, "Detection of Circumferential Cracks in Heat Exchanger Tubes Using Pulsed Eddy Current Testing," NDT&E Int., 121(1), p. 102444.
- [12] Ge, J., Yusa, N., and Fan, M., 2021, "Frequency Component Mixing of Pulsed or Multifrequency Eddy Current Testing for Nonferromagnetic Plate Thickness Measurement Using a Multigene Genetic Programming Algorithm," NDT&E Int., 120(1), p. 102423.
- [13] Lu, M., Meng, X., Huang, R., Chen, L., Peyton, A., Yin, W., and Qu, Z., 2021, "Thickness Measurement of Circular Metallic Film Using Single-Frequency Eddy Current Sensor," NDT&E Int., 119(6), p. 102420.
- [14] Tian, G. Y., Sophian, A., Taylor, D., and Rudlin, J., 2005, "Multiple Sensors on Pulsed Eddy-Current Detection for 3-D Subsurface Crack Assessment," IEEE Sens. J., 5(1), pp. 90–96.
- [15] Dogaru, T., and Smith, S. T., 2001, "Giant Magnetoresistance-Based Eddy-Current Sensor," IEEE Trans. Magn., 37(5), pp. 3831–3838.
- [16] Shull, P. J., Clark, A. V., and Auld, B. A., 1989, "Applications of Capacitive Array Sensors to Nondestructive Evaluation," *Nondestructive Characterization* of Materials, Springer, Berlin, pp. 582–589.
- [17] Kumar, R., Lang, J. H., Hamer, T., and Trumper, D. L., 2016, "Towards High-Bandwidth Capacitive Imaging," 2016 IEEE SENSORS, Orlando, FL, Oct. 30–Nov. 2, IEEE, Silver Spring, MD, pp. 1–3.
- [18] Martinsen, K., Hu, S. J., and Carlson, B. E., 2015, "Joining of Dissimilar Materials," CIRP Ann., 64(2), pp. 679–699.
- [19] Krishnan, P. K., Arunachalam, R., Husain, A., and Al-Maharbi, M., 2021, "Studies on the Influence of Stirrer Blade Design on the Microstructure and Mechanical Properties of a Novel Aluminum Metal Matrix Composite," ASME J. Manuf. Sci. Eng., 143(2), p. 021008.
- [20] Rojas, J. A., Ribeiro, B., and Rezende, M. C., 2021, "Curing of Glass Fiber/Epoxy Resin Composites Using Multiwalled Carbon Nanotubes Buckypaper as a Resistive Element," ASME J. Manuf. Sci. Eng., 143(4), p. 041007.
- [21] Cheng, J., Qiu, J., Xu, X., Ji, H., Takagi, T., and Uchimoto, T., 2016, "Research Advances in Eddy Current Testing for Maintenance of Carbon Fiber Reinforced Plastic Composites," Int. J. Appl. Electromagn. Mech., 51(3), pp. 261–284.
- [22] Kim, D., Kim, S., Kong, H. J., and Lee, Y., 2002, "Measurement of the Thickness Profile of a Transparent Thin Film Deposited Upon a Pattern Structure With an Acousto-Optic Tunable Filter," Opt. Lett., 27(21), pp. 1893–1895.
- [23] Stepinski, T., and Jonsson, M., 2005, "Narrowband Ultrasonic Spectroscopy for NDE of Layered Structures," Insight: Non-Destr. Test. Cond. Monit., 47(4), pp. 220–225.
- [24] Stepinski, T., 2006, "Assessing Quality of Self-Piercing Rivets Using Ultrasound," European Conference on Non-Destructive Testing, Berlin, Germany, Sept. 26–29.
- [25] Johnson, P., Cullen, J. D., Al-Shamma'a, A. I., and Shaw, A., 2007, "Online Visual Inspection of Self-Piercing Riveting to Determine the Quality of the Mechanical Interlock," J. Phys. Conf. Ser., 76(1), p. 012012.
- [26] He, X., Pearson, I., and Young, K., 2008, "Self-Pierce Riveting for Sheet Materials: State of the Art," J. Mater. Process. Technol., 199(1-3), pp. 27-36.
- [27] Li, D., Chrysanthou, A., Patel, I., and Williams, G., 2017, "Self-Piercing Riveting—A Review," Int. J. Adv. Manuf. Technol., 92(5), pp. 1777–1824.
- [28] Pappas, J. M., Thakur, A. R., Leu, M. C., and Dong, X., 2021, "A Comparative Study of Pellet-Based Extrusion Deposition of Short, Long, and Continuous Carbon Fiber-Reinforced Polymer Composites for Large-Scale Additive Manufacturing," ASME J. Manuf. Sci. Eng., 143(7), p. 071012.
- [29] Gay, A., Roche, J. M., Lapeyronnie, P., Valiorgue, F., and Bertrand, P., 2017, "Non-Destructive Inspection of Initial Defects of PA6. 6-GF50/Aluminum Self-Piercing Riveted Joints and Damage Monitoring Under Mechanical Static Loading," Int. J. Damage Mech., 26(8), pp. 1127–1146.